crystals

MDPI

Article

Entropy Generation Incorporating γ-Nanofluids under the Influence of Nonlinear Radiation with Mixed Convection

Umair Khan [1], Aurang Zaib [2], Ilyas Khan [3,*] and Kottakkaran Sooppy Nisar [4]

[1] Department of Mathematics and Social Sciences, Sukkur IBA University, Sukkur 65200, Pakistan; umairkhan@iba-suk.edu.pk
[2] Department of Mathematical Sciences, Federal Urdu University of Arts, Science & Technology, Gulshan-e-Iqbal Karachi 75300, Pakistan; aurangzaib@fuuast.edu.pk
[3] Department of Mathematics, College of Science Al-Zulfi, Majmaah University, Al-Majmaah 11952, Saudi Arabia
[4] Department of Mathematics, College of Arts and Science, Prince Sattam bin Abdulaziz University, Wadi Al-Dawaser 11991, Saudi Arabia; n.sooppy@psau.edu.sa
* Correspondence: i.said@mu.edu.sa

Abstract: Nanofluids offer the potential to improve heat transport performance. In light of this, the current exploration gives a numerical simulation of mixed convection flow (MCF) using an effective Prandtl model and comprising water- and ethylene-based $\gamma - Al_2O_3$ particles over a stretched vertical sheet. The impacts of entropy along with non-linear radiation and viscous dissipation are analyzed. Experimentally based expressions of thermal conductivity as well as viscosity are utilized for $\gamma - Al_2O_3$ nanoparticles. The governing boundary-layer equations are stimulated numerically utilizing bvp4c (boundary-value problem of fourth order). The outcomes involving flow parameter found for the temperature, velocity, heat transfer and drag force are conferred via graphs. It is determined from the obtained results that the temperature and velocity increase the function of the nanoparticle volume fraction for $H_2O \backslash C_2H_6O_2$ based $\gamma - Al_2O_3$ nanofluids. In addition, it is noted that the larger unsteady parameter results in a significant advancement in the heat transport and friction factor. Heat transfer performance in the fluid flow is also augmented with an upsurge in radiation.

Keywords: time-dependent flow; entropy generation; non-linear radiation; γ-alumina nanoparticle; MHD; mixed convection

check for updates

Citation: Khan, U.; Zaib, A.; Khan, I.; Nisar, K.S. Entropy Generation Incorporating γ-Nanofluids under the Influence of Nonlinear Radiation with Mixed Convection. *Crystals* **2021**, *11*, 400. https://doi.org/10.3390/cryst11040400

Academic Editors: Rajratan Basu and Arcady Zhukov

Received: 26 February 2021
Accepted: 31 March 2021
Published: 10 April 2021

1. Introduction

Several industrial processes, such as the growing of crystals, the manufacture of rubber and plastic sheets, paper and glass fiber production, and processes of polymer and metal extrusion are affected by the flow problem with heat transport provoked through stretched sheets; thus, this issues is extremely important. The cooling rate plays a significant role concerning the quality of the finished product through these procedures; where a moving sheet materializes via an incision, as a result, a boundary layer flow (BLF) emerges in the track of the surface progress. Crane [1] scrutinized the 2D steady flow of viscous fluid from a stretched sheet. After this study, the pioneering effort on the flow field through a stretched sheet achieved substantial interest; as a result, an excellent quantity of literature has been engendered on this work [2–9].

In recent times, nanotechnology has magnetized researchers' attention owing to its several distinct applications in the modern era, such as cancer therapy and diagnosis, interfaces in neuroelectronics, chemical production, and molecular and in vivo therapy applications such as kinesis and surgery, etc. In addition, there have been enhancements in the heat transfer in mechanical as well as thermal systems. Several regular fluids (ethylene glycol, oil, polymer solutions, water, etc.) have low thermal conductivity. Thus, augmenting the performance of such heat transport fluids appears imperative to achieve the expectations of scientists and researchers. Choi [10] primarily developed the concept of nanofluids for the purpose of augmenting the performance of regular fluids. Sheikholeslami et al. [11] scrutinized forced convective flow with nanofluids from a stretchable sheet with magnetic function. Mutuku and Makinde [12] examined the influences of dual stratification on time-dependent flow from a smooth sheet with nanofluid and magnetic function. The effect of entropy generation (EG) on the thin fluid flow with nanofluids via a stretched cylinder was scrutinized by Khan et al. [13]. Gireesha et al. [14] implemented a KVL (Khanafer-Vafai-Lightstone) model to explore the influence of nanofluids via dusty fluids with Hall effects. Recently, the influences of nanofluids rendering to assorted surfaces have been studied by numerous researchers [15–20].

The alumina nanofluids are another aspect that has recently attracted the attention of researchers due to their application in numerous procedures of cooling [21–26]. The alumina nanofluids are identified in accordance with their dimension, e.g., alpha and gamma aluminize, etc. The surface properties in well-described forms of gamma and eta alumina were examined in [27]. The entropy influence on the flow of ethylene- and water-based γ-alumina through stretched sheets, as determined using the effective Prandtl model, was explored by Rashidi et al. [28]. The authors claimed that the fluid temperature decelerates owing to effective Pr and accelerates without effective Pr. A comparative investigation considering $\gamma - Al_2O_3$ with distinct base fluids was scrutinized by Ganesh et al. [29]. They showed that similar nanoparticles have opposite effects on temperature. Moghaieb et al. [30] employed the $\gamma - Al_2O_3$ particles in their research as an engine coolant. Ahmed et al. [31] examined the unsteady radiative flow comprising ethylene- and water-based $\gamma - Al_2O_3$ nanomaterials through a thin slit with magnetic function. Recently, Zaib et al. [32] developed the model of effective Prandtl to examine the mixed convective flow through a wedge by nanofluids. They achieved multiple results for the opposite flow.

The second law of thermodynamics is more consistent than the first law of thermodynamics because of the restriction of the effectiveness of the first law in engineering systems of heat transport. To find the best method for thermal structures, the second law is employed through the curtailing of irreversibility [33,34]. A larger entropy generation (EG) signifies a larger scope of irreversibility. Hence, EG can be utilized to ascertain criteria for the manufacturing of devices in engineering. An assessment of EG can be used to augment the performance of a system [35–41]. In addition, entropy generation can be utilized in analysis of the brain and its diseases from both a psychiatric as well as a neurological perspective. Rashidi et al. [42] examined the stimulus of magnetic function on the fluid flow in a rotated permeable disk with nanofluid. Dalir et al. [43] surveyed the effect of entropy on the force convective flow from a stretching surface containing viscoelastic nanofluid. The Keller-box algorithm was utilized to find the numerical result. Shit et al. [44] discussed the effect of EG on convective magneto flow using nanofluid in porous medium with radiation impact. They employed FDM (finite difference method) along with Newton's technique of linearization. The influences of radiation and viscous dissipation on the flow of copper and silver nanomaterials through a rotated disk with entropy were studied by Hayat et al. [45]. Recently, Shafee et al. [46] scrutinized the stimulus of nanofluid via a tube with entropy generation by involving swirl tools of the flow.

The above-mentioned investigations were dependent on steady- state behavior. However, in certain situations, the flow depends on time, owing to unexpected changes in temperature or the heat-flux of the surface, and as a result, it becomes vital to take time-dependent (unsteady) flow conditions into consideration. In addition, the phenomena of time-dependent flow is significant in numerous areas of engineering, such as rotating parts in piston engines, the turbo machinery and aerodynamics of helicopters, etc. Thus, the intention of the current research is to explore the impact of time-dependent mixed convective flow incorporating $H_2O\backslash C_2H_6O_2$ based γ-nanofluids. The influences of nonlinear radiation and viscous dissipation with entropy are also analyzed. The Lobatto IIIA formula is used to find the numerical solutions of the transmuted ODEs (ordinary differential equations).

2. Mathematical Formulation

In the mathematical model presented herein, we incorporated the time-dependent 2D mixed convective flow of $H_2O \backslash C_2H_6O_2$ based $\gamma - Al_2O_3$ nanoparticles through a stretched vertical sheet. The viscous dissipation, non-linear radiation and non-uniform heat source/sink were taken as an extra assumption in the energy equation. It was also presumed that the flow was incompressible and that the nanoparticles and the base fluid were in thermal equilibrium. The applied magnetic field (MF) was taken to be time-dependent $B = B_0/\sqrt{1 - Ct}$ and normal to the flow of surface. In addition, there was no polarization effect, and thus the external electric field was presumed to be zero and the magnetic Reynolds number was presumed to be small (in comparison to the applied MF, the induced MF was negligible). The demarcated values of the thermo-physical properties of the aforementioned nanofluids are shown in Table 1.

Table 1. Thermo-physical properties of nanoparticle and base fluids [47].

	Water (H_2O)	**Ethylene Glycol ($C_2H_6O_2$)**	**Alumina (Al_2O_3)**
ρ' (kg/m^3)	998.3	1116.6	3970
c'_p (J/kg, K)	4182	2382	765
k' (W/m, K)	0.60	0.249	40
$\beta' \times 10^{-5}$ (K^{-1})	20.06	65	0.85
σ' $(\Omega, \mathrm{m})^{-1}$	0.05	1.07×10^{-7}	10^{-12}
Pr	6.96	204	-

The coordinate system is assumed in Cartesian form (x, y, t), where the x-axis is run along the stretching sheet and the y-axis is orthogonal to it; t symbolizes the time. The velocity and temperature at the stretching sheet are respectively presented as $U_w = ax/(1 - Ct)$ and $T_f = T_\infty + bx^2/(1 - Ct)^2$, where a, b, are the constants and the capital letter C is used for the decelerated and accelerated sheet when $C < 0$ and $C > 0$, respectively. Under these hypotheses, the governing equations for the momentum and heat transfer of nanofluids with thermo-physical properties and unsteady boundary layer convective flow can be explained as:

$$\frac{\partial u_1}{\partial x} + \frac{\partial v_1}{\partial y} = 0 \tag{1}$$

$$\frac{\partial u_1}{\partial t} + v_1 \frac{\partial u_1}{\partial y} + u_1 \frac{\partial u_1}{\partial x} = \frac{\mu'_{nf}}{\rho'_{nf}} \frac{\partial^2 u_1}{\partial y^2} - \frac{\sigma'_{nf} B^2}{\rho'_{nf}} u_1 + g' \frac{(\rho' \beta')_{nf}}{\rho'_{nf}} (T_1 - T_\infty) \tag{2}$$

$$\frac{\partial T_1}{\partial t} + v_1 \frac{\partial T_1}{\partial y} + u_1 \frac{\partial T_1}{\partial x} = \frac{k'_{nf}}{(\rho' c'_p)_{nf}} \frac{\partial^2 T_1}{\partial y^2} - \frac{1}{(\rho' c'_p)_{nf}} \left(\frac{\partial q'_r}{\partial y} \right) + \frac{\mu'_{nf}}{(\rho' c'_p)_{nf}} \left(\frac{\partial u_1}{\partial y} \right)^2 + \frac{Q_0}{(\rho' c'_p)_{nf}} \tag{3}$$

The approximation of Rosseland for the term nonlinear radiative heat flux is given as:

$$q'_r = -\frac{4\sigma'^*}{3k'^*} \frac{\partial T_1^4}{\partial y} = -\frac{16\sigma'^*}{3k'^*} T_1^3 \frac{\partial T_1}{\partial y} \tag{4}$$

Utilizing Equation (4) in Equation (3), it can defined as:

$$\frac{\partial T_1}{\partial t} + v_1 \frac{\partial T_1}{\partial y} + u_1 \frac{\partial T_1}{\partial x} = \frac{k'_{nf}}{(\rho' c'_p)_{nf}} \frac{\partial^2 T_1}{\partial y^2} + \frac{16\sigma'^* T_1^2}{3k'^* (\rho' c'_p)_{nf}} \left(T_1 \frac{\partial}{\partial y} \left(\frac{\partial T_1}{\partial y} \right) + 3 \left(\frac{\partial T_1}{\partial y} \right)^2 \right) + \frac{\mu'_{nf}}{(\rho' c'_p)_{nf}} \left(\frac{\partial u_1}{\partial y} \right)^2 + \frac{Q_0}{(\rho' c'_p)_{nf}}, \tag{5}$$

where the last term represents the erratic heat sink/source and is defined as:

$$Q_0 = \frac{k'_f\left(T_f - T_\infty\right)U_w(x,t)}{x\nu'_f}\left(A_0 f' + B_0\left(\frac{T_1 - T_\infty}{T_f - T_\infty}\right)\right) \tag{6}$$

The boundary conditions are:

$$\begin{gathered} -k'_{nf}\frac{\partial T_1}{\partial y} = h_f\left(T_f - T_1\right), u_1 = U_w(x,t),\ v_1 = 0,\ \text{at } y = 0, \\ T_1 \to T_\infty, u_1 \to 0 \text{ as } y \to \infty. \end{gathered} \tag{7}$$

Here, T_1 is the temperature, T_∞ is the free stream or the cold temperature moving on the right side of the sheet, with a zero free stream velocity, while the left side of the sheet is heated at temperature T_f from a hot fluid owing convection, which offers a coefficient of heat transfer h_f and comprising the expression of thermo-physical properties revealed in Table 2. The interpretations of the rest of the symbols or notations and the mathematical letters in Equation (1) to Equation (7) are presented in Table 3.

Table 2. Thermo-physical properties of gamma nanofluids.

	Symbols	Expressions	Model
Effective dynamic viscosity	μ'_{nf}/μ'_f	$123\phi^2 + 7.3\phi + 1$	$\gamma Al_2O_3{-}H_2O$
Effective dynamic viscosity	μ'_{nf}/μ'_f	$306\phi^2 - 0.19\phi + 1$	$\gamma Al_2O_3{-}C_2H_6O_2$
Effective thermal conductivity	k'_{nf}/k'_f	$4.97\phi^2 + 2.72\phi + 1$	$\gamma Al_2O_3{-}H_2O$
Effective thermal conductivity	k'_{nf}/k'_f	$28.905\phi^2 + 2.8273\phi + 1$	$\gamma Al_2O_3{-}C_2H_6O_2$
Effective Prandtl number	Pr_{nf}/Pr_f	$82.1\phi^2 + 3.95\phi + 1$	$\gamma Al_2O_3{-}H_2O$
Effective Prandtl number	Pr_{nf}/Pr_f	$254.3\phi^2 - 3\phi + 1$	$\gamma Al_2O_3{-}C_2H_6O_2$
Effective dynamic density	ρ'_{nf}	$(1-\phi)\rho'_f + \phi\rho'_s$	
Heat capacitance	$(\rho' c'_p)_{nf}$	$(1-\phi)(\rho' c'_p)_f + \phi(\rho' c'_p)_s$	
Thermal expansion	$(\rho'\beta')_{nf}$	$(1-\phi)(\rho'\beta')_f + \phi(\rho'\beta')_s$	
Electrical conductivity	σ'_{nf}/σ'_f	$\left\{1 + \frac{3(\sigma'_s/\sigma'_f - 1)}{(\sigma'_s/\sigma'_f + 2) - \phi(\sigma'_s/\sigma'_f - 1)}\right\}$	

Following the non-dimensional similarity variables are:

$$\begin{gathered} u_1 = ax(1-Ct)^{-0.5}F',\ v_1 = -\left(v'_f a(1-Ct)^{-0.5}\right)^{\frac{1}{2}}F, \\ \eta = y\left(\frac{a(1-Ct)^{-0.5}}{v'_f}\right)^{\frac{1}{2}},\ \theta = \frac{T_1 - T_\infty}{T_f - T_\infty}. \end{gathered} \tag{8}$$

Using Equation (8) in Equation (2) to Equation (6), along with the boundary condition (7) we get the dimensional form of the momentum equations, as follows:

$$\left.\begin{aligned} K_1 F''' + \left[K_2\left(FF'' - F'^2 - \varepsilon\left(\tfrac{\eta}{2}F'' + F'\right)\right) - K_3 MF' + K_4\lambda\theta\right] = 0 \\ (\text{for } \gamma Al_2O_3 - H_2O) \end{aligned}\right\} \tag{9}$$

$$\left.\begin{aligned} K_5 F''' + \left[K_2\left(FF'' - F'^2 - \varepsilon\left(\tfrac{\eta}{2}F'' + F'\right)\right) - K_3 MF' + K_4\lambda\theta\right] = 0 \\ (\text{for } \gamma Al_2O_3 - C_2H_6O_2) \end{aligned}\right\}, \tag{10}$$

Table 3. The list of symbols used and their interpretation.

Symbols	Interpretation
$(u_1(x,y,t), v_1(x,y,t), 0)$	Velocity components
(x,y)	Cartesian Coordinates
t	Time
F	Dimensionless velocity
B	Magnetic number
$A_0 > 0, B_0 > 0$	Heat source
$A_0 < 0, B_0 < 0$	Heat sink
g'	Gravitational acceleration
Greek Symbols	**Interpretation**
${\mu'}_{nf}$	Dynamic viscosity of nanofluid
${\rho'}_{nf}$	Density of nanofluid
${\sigma'}_{nf}$	Electrical conductivity of nanofluid
$(\rho'\beta')_{nf}$	Thermal expansion of nanofluid
$(\rho'{c'}_p)_{nf}$	Heat capacity of nanofluid
${k'}_{nf}$	Thermal conductivity of nanofluid
${\nu'}_f$	Kinematic viscosity
${\sigma'}^*$	Stefan Boltzmann constant
${k'}^*$	Mean absorption constant
$\theta(\eta)$	Dimensionless temperature
ϕ	Nanoparticle volume fraction
Subscript	**Interpretation**
nf	Nanofluid

In which:

$$\mathrm{K}_1 = \left(123\phi^2 + 7.3\phi + 1\right), \mathrm{K}_2 = \left(1 - \phi + \phi\left(\frac{{\rho'}_s}{{\rho'}_f}\right)\right), \mathrm{K}_3 = \left[\frac{3\phi\left(\frac{{\sigma'}_s}{\sigma_f} - 1\right)}{\left(\frac{{\sigma'}_s}{{\sigma'}_f} + 2\right) - \left(\frac{{\sigma'}_s}{{\sigma'}_f} - 1\right)\phi} + 1\right],$$
$$\mathrm{K}_4 = (1 - \phi) + \phi\frac{(\rho'\beta')_s}{(\rho'\beta')_f}, \mathrm{K}_5 = \left(306\phi^2 - 0.19\phi + 1\right).$$

while the corresponding dimensional form of the energy equations for the γAl_2O_3 nanoparticle are given as:

$$\left.\begin{array}{r} \theta''\left[1 + \frac{4}{3}R_d\mathrm{K}_6(1 + (\theta_w - 1)\theta)^3\right] + 4R_d\mathrm{K}_6\left[(1 + (\theta_w - 1)\theta)^2\theta'^2(\theta_w - 1)\right] + \\ \mathrm{K}_7\left\{(F\theta' - 2F'\theta) - \varepsilon\left(2\theta + \frac{\eta}{2}\theta'\right)\right\} + \mathrm{K}_6(A_0F' + B_0\theta) + \mathrm{Pr}_f\mathrm{K}_1 Ec(F'')^2 = 0 \\ (\text{for } \gamma\mathrm{Al}_2\mathrm{O}_3 - \mathrm{H}_2\mathrm{O}) \end{array}\right\}, \quad (11)$$

$$\left.\begin{array}{r} \theta''\left[1 + \frac{4}{3}R_d\mathrm{K}_8(1 + (\theta_w - 1)\theta)^3\right] + 4R_d\mathrm{K}_8\left[(1 + \theta(\theta_w - 1))^2\theta'^2(\theta_w - 1)\right] + \\ \mathrm{K}_9\left\{(F\theta' - 2F'\theta) - \varepsilon\left(2\theta + \frac{\eta}{2}\theta'\right)\right\} + \mathrm{K}_8(A_0F' + B_0\theta) + \mathrm{Pr}_f\mathrm{K}_5 Ec(F'')^2 = 0 \\ (\text{for } \gamma\mathrm{Al}_2\mathrm{O}_3 - \mathrm{C}_2\mathrm{H}_6\mathrm{O}_2) \end{array}\right\}, \quad (12)$$

and the appropriate boundary conditions are:

$$\left.\begin{array}{l}\theta'(0) = -\mathrm{K}_6\xi(1-\theta(0)),\ F'(0) = 1,\ F(0) = 0 \text{ at } \eta = 0,\\ \theta(\eta) \to 0,\ F'(\eta) \to 0 \text{ as } \eta \to \infty.\\ \hfill (\text{for } \gamma\mathrm{Al_2O_3} - \mathrm{H_2O})\end{array}\right\}, \tag{13}$$

$$\left.\begin{array}{l}\theta'(0) = -\mathrm{K}_8\xi(1-\theta(0)),\ F'(0) = 1,\ F(0) = 0 \text{ at } \eta = 0,\\ \theta(\eta) \to 0,\ F'(\eta) \to 0,\ \text{ as } \eta \to \infty.\\ \hfill (\text{for } \gamma\mathrm{Al_2O_3} - \mathrm{C_2H_6O_2})\end{array}\right\}. \tag{14}$$

Where:

$$\mathrm{K}_6 = \frac{1}{4.97\phi^2+2.72\phi+1},\ \mathrm{K}_7 = \frac{\mathrm{Pr}_f\left(1-\phi+\phi\left(\frac{\rho'_s}{\rho'_f}\right)\right)\left(82.1\phi^2+3.95\phi+1\right)}{123\phi^2+7.3\phi+1},$$

$$\mathrm{K}_8 = \frac{1}{28.905\phi^2+2.8273\phi+1},\ \mathrm{K}_9 = \frac{\mathrm{Pr}_f\left(1-\phi+\phi\left(\frac{\rho'_s}{\rho'_f}\right)\right)\left(254.3\phi^2-3\phi+1\right)}{306\phi^2-0.19\phi+1}.$$

For the above equations, the interpretations of the various dimensional parameters are given in Table 4 (for Equation (9) to Equation (14)). The remaining two parameters are the local mixed convection parameter (ratio of the Grashof number and Reynolds number) and the convective parameter and are demarcated as follows:

$$\begin{array}{l}\lambda = \frac{Gr_x}{\mathrm{Re}^2{}_x},\ \mathrm{Re}_x = \frac{xU_w}{\nu'_f},\\ Gr_x = g'\beta'_f\left(T_f - T_\infty\right)x^3/\nu'^2{}_f,\ Bi = \frac{h_f\sqrt{\nu'_f}(1-Ct)}{k'_f\sqrt{a}}\end{array} \tag{15}$$

Table 4. The list of parameters used and their values.

Name of Parameter	Notation/Symbols	Values
Magnetic parameter	M	$\sigma'_f B_0^2/\rho'_f a$
Unsteadiness parameter	ε	C/a
Radiation parameter	R_d	$4\sigma'^* T_\infty^3/k'_f k'^*$
Temperature ratio parameter	θ_w	T_f/T_∞
Eckert number	Ec	$\mu'_f U_w^2/(c'_p)_f\left(T_f - T_\infty\right)$

In order to find the similarity solution for Equations (9)–(12), it is presumed that [48]

$$\beta'_f = m_1 x^{-1} \text{ and } h_f = m_2(1-Ct)^{-0.5} \tag{16}$$

where m_1, m_2 are the constants.

Engineering Quantities of Interest

The friction factor and the temperature gradient in mathematical structure are described as:

$$C_F = \frac{\tau'_w}{\rho'_f U_w^2},\ Nu_x = \frac{xq'_w}{k'_f(T_f - T_\infty)}, \tag{17}$$

The wall shear stress and the heat-flux are expressed as:

$$\tau'_w = \mu'_{nf}\left(\frac{\partial u_1}{\partial y}\right)_{y=0},\ q'_w = -k'_f\left(\frac{k'_{nf}}{k'_f} + \frac{16\sigma'^* T_1^3}{3k'^* k'_f}\right)\left(\frac{\partial T_1}{\partial y}\right)_{y=0}. \tag{18}$$

Utilizing Equation (18) in Equation (17), the dimensionless expressions are:

$$\left.\begin{array}{r}C_F\mathrm{Re}_x^{0.5} = \mathrm{K}_1 F''(0) \\ Nu_x\mathrm{Re}_x^{-0.5} = -\left(\frac{1}{\mathrm{K}_6} + \frac{4}{3}R_d(1+(\theta_w-1)\theta(0))^3\right)\theta'(0) \\ (\text{for } \gamma\,\mathrm{Al_2O_3 - H_2O})\end{array}\right\} \tag{19}$$

$$\left.\begin{array}{r}C_F\mathrm{Re}_x^{0.5} = \mathrm{K}_5 F''(0) \\ Nu_x\mathrm{Re}_x^{-0.5} = -\left(\frac{1}{\mathrm{K}_8} + \frac{4}{3}R_d(1+(\theta_w-1)\theta(0))^3\right)\theta'(0) \\ (\text{for } \gamma\,\mathrm{Al_2O_3 - C_2H_6O_2})\end{array}\right\} \tag{20}$$

3. Formulation of Entropy

The volumetric EG (entropy generation) for $\gamma\mathrm{Al_2O_3}$ nanoparticles is expressed as:

$$H_G = \frac{k'_f}{T_\infty^2}\left[\frac{k'_{nf}}{k'_f} + \frac{16\sigma'^* T_1^3}{3k'^* k'_f}\right]\left(\frac{\partial T_1}{\partial y}\right)^2 + \frac{\mu'_{nf}}{T_\infty}\left(\frac{\partial u_1}{\partial y}\right)^2 + \frac{\sigma'_{nf}B^2}{T_\infty}u_1^2 \tag{21}$$

The characteristic EG rate can be written as:

$$H_{g0} = \frac{k'_f(\Delta T)^2}{L^2 T_\infty^2} \tag{22}$$

By using the ratio of Equations (21) and (22), the EG number is described as:

$$H_g = \frac{H_G}{H_{g0}} \tag{23}$$

Implementing Equation (8) in Equations (21) and (22), we obtain:

$$\left.\begin{array}{r}H_g = \mathrm{Re}_L\left(\frac{1}{\mathrm{K}_6} + \frac{4}{3}R_d(1+(\theta_w-1)\theta)^3\right)\theta'^2 + \frac{\mathrm{Re}_L Br}{\Omega}\mathrm{K}_1 F''^2 + \mathrm{K}_3\frac{MBr\mathrm{Re}_L}{\Omega}F'^2, \\ (\text{for } \gamma\mathrm{Al_2O_3 - H_2O})\end{array}\right\} \tag{24}$$

$$\left.\begin{array}{r}H_g = \mathrm{Re}_L\left(\frac{1}{\mathrm{K}_8} + \frac{4}{3}R_d(1+(\theta_w-1)\theta)^3\right)\theta'^2 + \frac{\mathrm{Re}_L Br}{\Omega}\mathrm{K}_5 F''^2 + K_3\frac{MBr\mathrm{Re}_L}{\Omega}F'^2, \\ (\text{for } \gamma\mathrm{Al_2O_3 - C_2H_6O_2})\end{array}\right\} \tag{25}$$

where the parameters $\Omega = \Delta T/T_\infty$, $Br = \mu'_f(U_w)^2/k'_f\Delta T$, $\mathrm{Re}_L = aL^2/\nu'_f(1-Ct)$ are described as the temperature difference and the Brinkman and Reynolds numbers, respectively.

The assessment of the Bejan Be number is vital in sequence to investigate the heat transfer irreversibility, and range of values is between 0 and 1. The Be number in dimensionless form is described as:

$$\left.\begin{array}{r}Be = \dfrac{\mathrm{Re}_L\left(\frac{1}{\mathrm{K}_6}+\frac{4}{3}R_d(1+(\theta_w-1)\theta)^3\right)\theta'^2}{\mathrm{Re}_L\left(\frac{1}{\mathrm{K}_6}+\frac{4}{3}R_d(1+(\theta_w-1)\theta)^3\right)\theta'^2+\frac{\mathrm{Re}_L Br}{\Omega}\mathrm{K}_1F''^2+\mathrm{K}_3\frac{MBr\mathrm{Re}_L}{\Omega}F'^2}, \\ (\text{for } \gamma\mathrm{Al_2O_3 - H_2O})\end{array}\right\} \tag{26}$$

$$\left.\begin{array}{r}Be = \dfrac{\mathrm{Re}_L\left(\frac{1}{\mathrm{K}_8}+\frac{4}{3}R_d(1+(\theta_w-1)\theta)^3\right)\theta'^2}{\mathrm{Re}_L\left(\frac{1}{\mathrm{K}_8}+\frac{4}{3}R_d(1+(\theta_w-1)\theta)^3\right)\theta'^2+\frac{\mathrm{Re}_L Br}{\Omega}\mathrm{K}_5F''^2+\mathrm{K}_3\frac{MBr\mathrm{Re}_L}{\Omega}F'^2}, \\ (\text{for } \gamma\mathrm{Al_2O_3 - C_2H_6O_2})\end{array}\right\} \tag{27}$$

It is concluded from the expressions mentioned above that the irreversibility of fluid friction dominates when Be differs from 0–0.5, while the heat transport irreversibility dominates when Be differs from 0.5–1. The value of Be demonstrates that the irreversibility of fluid friction and heat transfer equally contribute to EG.

4. Methodology

The momentum and energy coupled non-linear ODEs (Equations (9) and (10)) and (Equations (11) and (12)), along with the boundary conditions (BCs) in Equation (13) and Equation (14), are solved numerically via bvp4c in MATLAB, which is based on a three-stage Lobatto technique for the various comprising parameters and gamma nanofluids. The three-stage Lobatto technique is a collocation technique with fourth-order accuracy. The form of the ODEs (ordinary differential equations), along with the BCs, is altered into the group of first order IVP (intial value problem) by exercising the new variables. This process is carried forward by introducing the following variables:

$$F = Z_1,\ F' = Z_2,\ F'' = Z_3,\ \theta = Z_4,\ \theta' = Z_5, \tag{28}$$

Utilizing Equation (28) for the aforementioned ODEs and the boundary conditions, we get a system of ODEs for the model of $(\gamma Al_2O_3{-}H_2O)$ and $(\gamma Al_2O_3{-}C_2H_6O_2)$ nanofluids, respectively given as:

$$\frac{d}{d\eta}\begin{pmatrix} Z_1 \\ Z_2 \\ Z_3 \\ Z_4 \\ Z_5 \end{pmatrix} = \begin{pmatrix} Z_2 \\ Z_3 \\ \frac{-\left\{\mathrm{K}_2\left(Z_1Z_3 - Z_2Z_2 - \varepsilon\left(\frac{\eta}{2}Z_3 + Z_2\right)\right) - M\mathrm{K}_3Z_2 + \mathrm{K}_4\lambda Z_4\right\}}{\mathrm{K}_1} \\ Z_5 \\ \frac{\left\{\begin{array}{l} -4R_d\mathrm{K}_6(1+(\theta_w-1)Z_4)^2(\theta_w-1)Z_5Z_5 - \mathrm{K}_7\left((Z_1Z_5 - 2Z_2Z_4) - \varepsilon\left(2Z_4 + \frac{\eta}{2}Z_5\right)\right) - \\ \mathrm{K}_6(A_0Z_2 + B_0Z_4) - \mathrm{Pr}_f\,\mathrm{K}_1EcZ_3Z_3 \end{array}\right\}}{\left(1+\frac{4}{3}R_d\mathrm{K}_6(1+(\theta_w-1)Z_4)^3\right)} \end{pmatrix} \tag{29}$$

with initial conditions (ICs) as follows:

$$\begin{pmatrix} Z_1(0) \\ Z_2(0) \\ Z_2(\infty) \\ Z_5(0) \\ Z_4(\infty) \end{pmatrix} = \begin{pmatrix} 0 \\ 1 \\ 0 \\ -\mathrm{K}_6\xi(1 - Z_4(0)) \\ 0 \end{pmatrix}. \tag{30}$$

Similarly,

$$\frac{d}{d\eta}\begin{pmatrix} Z_1 \\ Z_2 \\ Z_3 \\ Z_4 \\ Z_5 \end{pmatrix} = \begin{pmatrix} Z_2 \\ Z_3 \\ \frac{-\left\{\mathrm{K}_2\left(Z_1Z_3 - Z_2Z_2 - \varepsilon\left(\frac{\eta}{2}Z_3 + Z_2\right)\right) - M\mathrm{K}_3Z_2 + \mathrm{K}_4\lambda Z_4\right\}}{\mathrm{K}_5} \\ Z_5 \\ \frac{\left\{\begin{array}{l} -4R_d\mathrm{K}_8(1+(\theta_w-1)Z_4)^2(\theta_w-1)Z_5Z_5 - \mathrm{K}_9\left((Z_1Z_5 - 2Z_2Z_4) - \varepsilon\left(2Z_4 + \frac{\eta}{2}Z_5\right)\right) - \\ \mathrm{K}_8(A_0Z_2 + B_0Z_4) - \mathrm{Pr}_f\,\mathrm{K}_5EcZ_3Z_3 \end{array}\right\}}{\left(1+\frac{4}{3}R_d\mathrm{K}_8(1+(\theta_w-1)Z_4)^3\right)} \end{pmatrix}, \tag{31}$$

with the corresponding (ICs) as follows:

$$\begin{pmatrix} Z_1(0) \\ Z_2(0) \\ Z_2(\infty) \\ Z_5(0) \\ Z_4(\infty) \end{pmatrix} = \begin{pmatrix} 0 \\ 1 \\ 0 \\ -\mathrm{K}_8\xi(1 - Z_4(0)) \\ 0 \end{pmatrix}. \tag{32}$$

The use of an efficient estimation for $F''(0)$ and $\theta'(0)$ until the boundary restriction is reached addresses these equations. The step size is fixed to $\Delta\eta = 0.01$, which is sufficient to achieve the graphical and the numerical result in tabular form. The range is taken to be $\eta_{\max} = 10$, where the finite value of the dimensional variable η for the boundary restrictions is $\eta_{\max}$. The convergence criteria and the accuracy of the outcomes in all cases are up to level 10^{-10}.

5. Results and Discussion

The impacts of numerous pertinent parameters on the temperature, velocity, heat transfer and drag force are discussed and presented in tabular form and as well as graphically (see Figures 1–21). Table 5 shows the assessment of $-F''(0)$ with current outcomes through the outcomes reported by Shafie [49] and Chamkha [50].

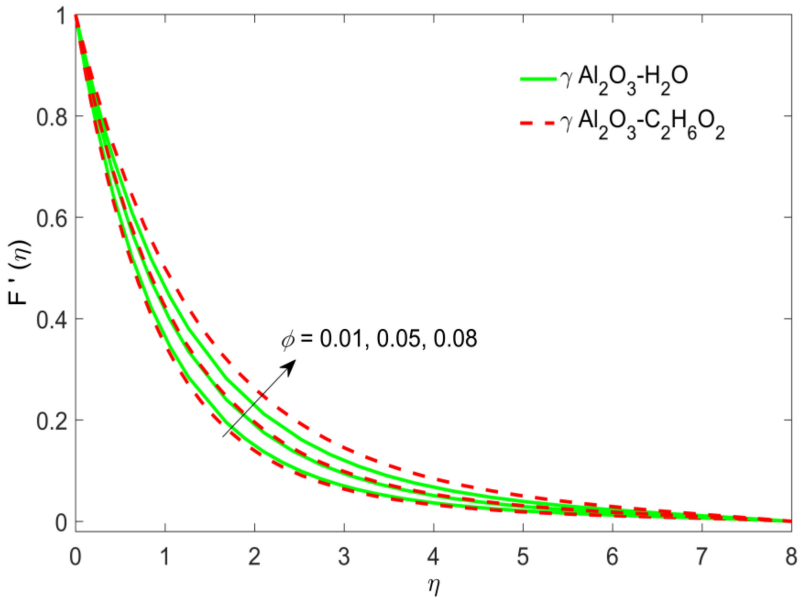

Figure 1. Impact of ϕ on $F'(\eta)$.

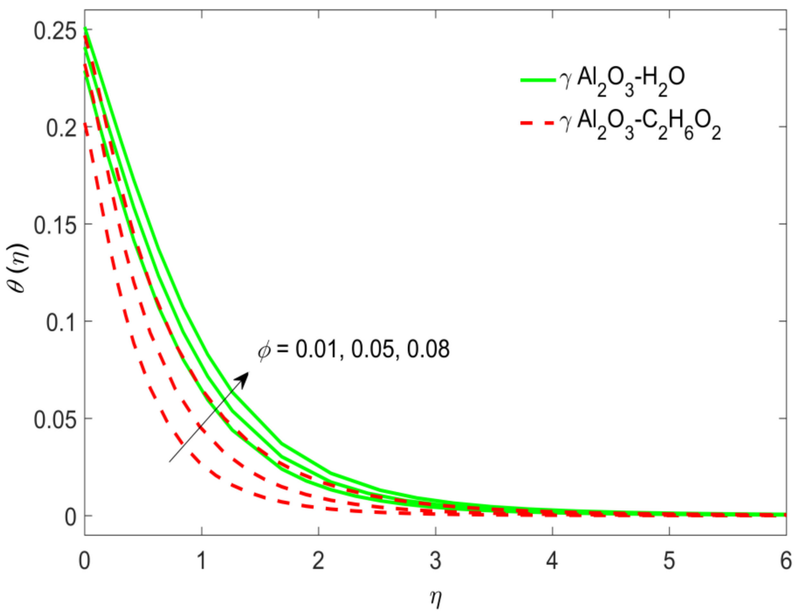

Figure 2. Impact of ϕ on $\theta(\eta)$.

The outcomes depict a superb conformity. The significant parameters for computational purposes are considered as $\phi = 0.02,\ M = 0.1,\ \varepsilon = 10,\ \xi = 0.5,\ \theta_w = 0.1,\ Ec = 0.5,$ $A_0 = B_0 = 0.1$ and $R_d = 02$, with the variations shown in Figures 1–21.

Figures 1 and 2 describe the influence of volume fraction ϕ on the velocity $F'(\eta)$ and fluid temperature $\theta(\eta)$. Figures 1 and 2 confirm that the $F'(\eta)$ and $\theta(\eta)$ accelerate gradually for larger values of ϕ. Physically, the nanofluid density under consideration decreases due to the larger amount of ϕ, which consequently augments the velocity and temperature. Thus, the inter-molecular forces between the particles of nanofluids become weaker, and as a result, the fluid velocity accelerates. It is also clear from Figure 2 that the temperature is higher in the case of water and lower in case of ethylene glycol. The justification for this result is that water has a smaller Prandtl number than ethylene glycol, and as a result, the water thermal diffusivity is much superior to that of ethylene glycol. In addition, $C_2H_6O_2$ nanoliquids can be utilized for the purpose of cooling.

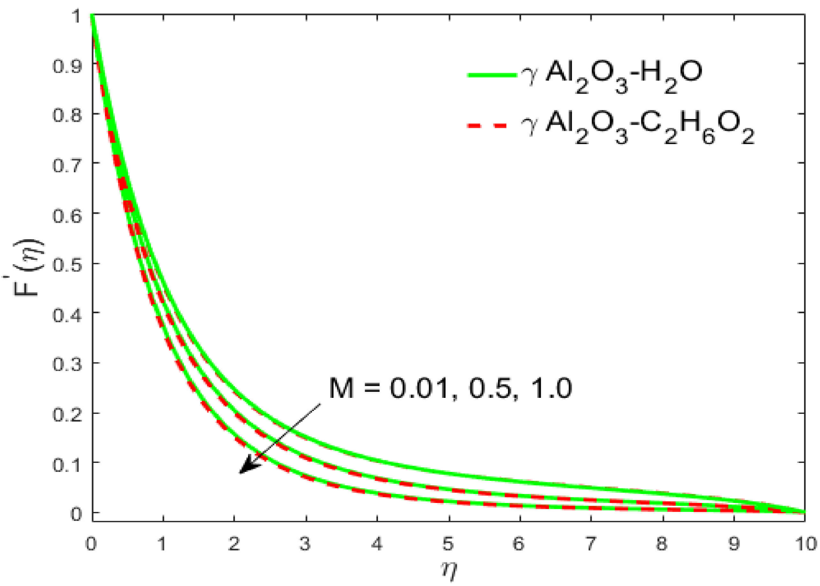

Figure 3. Impact of M on $F'(\eta)$.

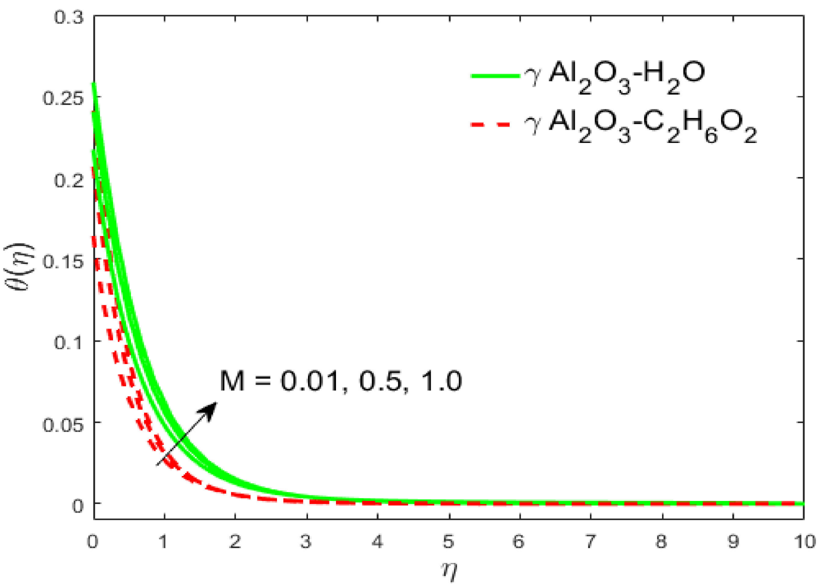

Figure 4. Impact of M on $\theta(\eta)$.

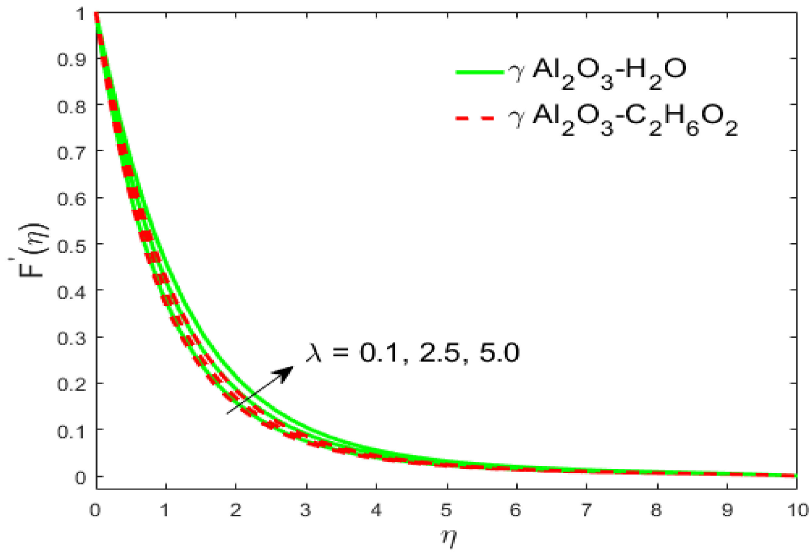

Figure 5. Impact of $\lambda > 0$ on $F'(\eta)$.

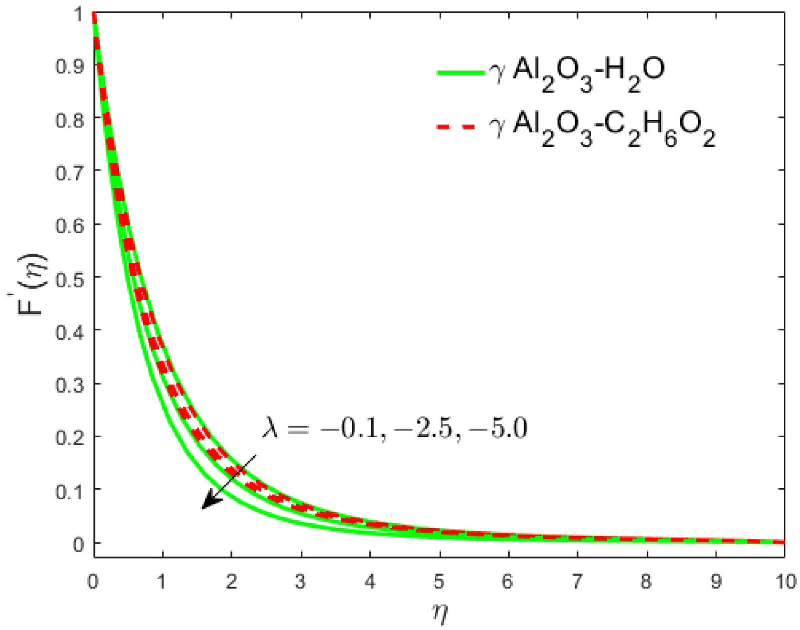

Figure 6. Impact of $\lambda < 0$ on $F'(\eta)$.

Table 5. Comparison of the values of $-F''(0)$, when $M = \phi = \lambda = 0$.

ε	Shafie et al. [49]	Chamkha et al. [50]	Current Results
0.8	1.261042	1.261512	1.2610
1.2	1.377722	1.378052	1.3777

The influence of M on $F'(\eta)$ and $\theta(\eta)$ is portrayed in Figures 3 and 4. Figure 3 suggests that the velocity declines due to M in both $H_2O\backslash C_2H_6O_2$ based nanofluids.

Physically, the existence of magnetic function engenders a type of resistive force (or Lorentz force) in the flow region, which holds the nanofluid motion. In contrast, the temperature profile (Figure 4) rises as a result of M. The physics behind this are that an enhancement in magnetic function causes an upsurge in electro-magnetic force, which controls the motion of fluid and consequently increases the temperature as well as the thickness. Figures 5–8 show the impact of λ on $F'(\eta)$ and $\theta(\eta)$ for assisting and opposing flows.

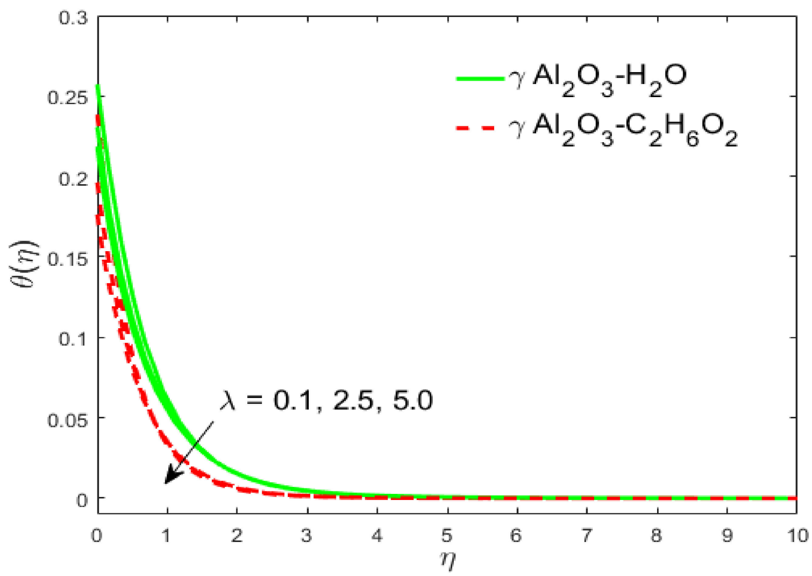

Figure 7. Impact of $\lambda > 0$ on $\theta(\eta)$.

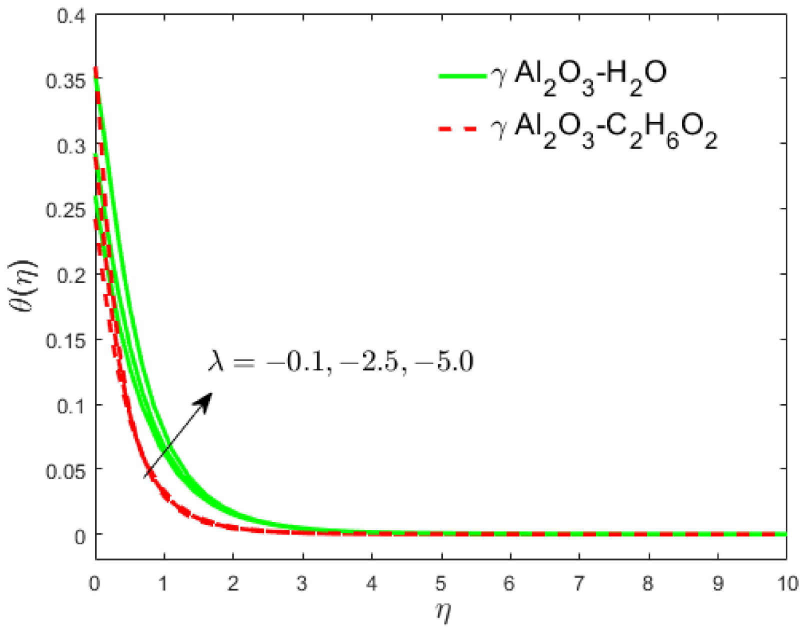

Figure 8. Impact of $\lambda < 0$ on $\theta(\eta)$.

It is clear from Figure 5 that the velocity increases with λ in the assisting flow, while the velocity as shown in Figure 6 declines in the opposing flow. Physically, a greater amount of λ generates a substantial buoyancy force that ultimately generates greater kinetic energy. The reverse is true for the opposing flow. Figure 7 shows that the temperature diminishes due to λ for assisting flow in both $\gamma Al_2O_3 - H_2O$ and $\gamma Al_2O_3 - C_2H_6O_2$ nanofluids, whereas the temperature increases in the opposing flow, as depicted in Figure 8. Physically, the fluid attains the heat from the sheet, and later on, heat energy is transmuted into different forms of energy, like kinetic energy. As expected, the temperature is lower for $\gamma Al_2O_3 - C_2H_6O_2$ than $\gamma Al_2O_3 - H_2O$ due to the greater Prandtl number. The nature of the temperature profiles is observed in Figures 9–11 for changed values of R_d, Ec and ξ.

Figure 9 confirms that temperature increases with R_d for $H_2O\backslash C_2H_6O_2$ based $\gamma - Al_2O_3$ nanofluids. The coefficient of absorption declines as radiation increases, and due to this, an enhancement occurs in the temperature distribution. Similar behavior is noticed for the Eckert number, owing to fractional heating as illustrated in Figure 10. Larger inference of Ec implies that the heat of thermal dissipation is stocked in the fluid, which ultimately increases the temperature. The convective parameter causes upsurges in the distribution of temperature (Figure 11) for $H_2O\backslash C_2H_6O_2$ based $\gamma - Al_2O_3$ nanofluids.

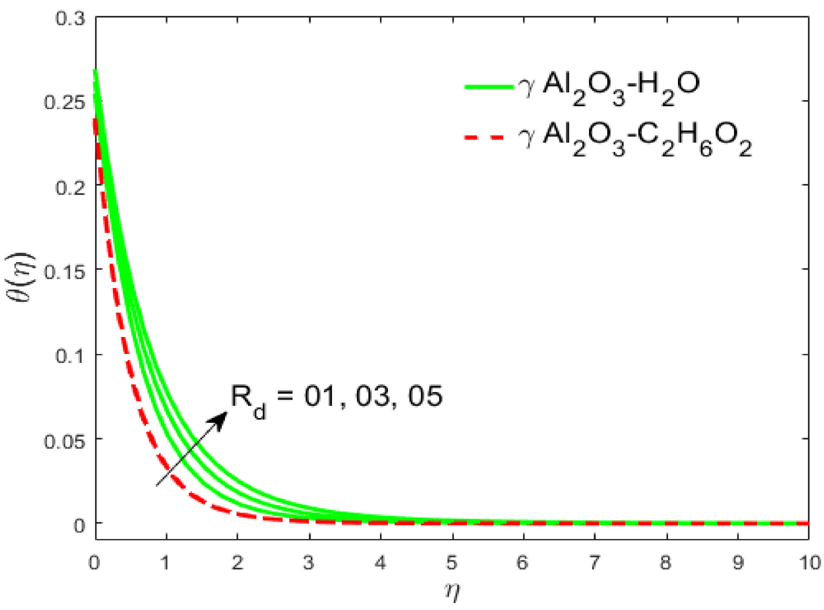

Figure 9. Impact of R_d on $\theta(\eta)$.

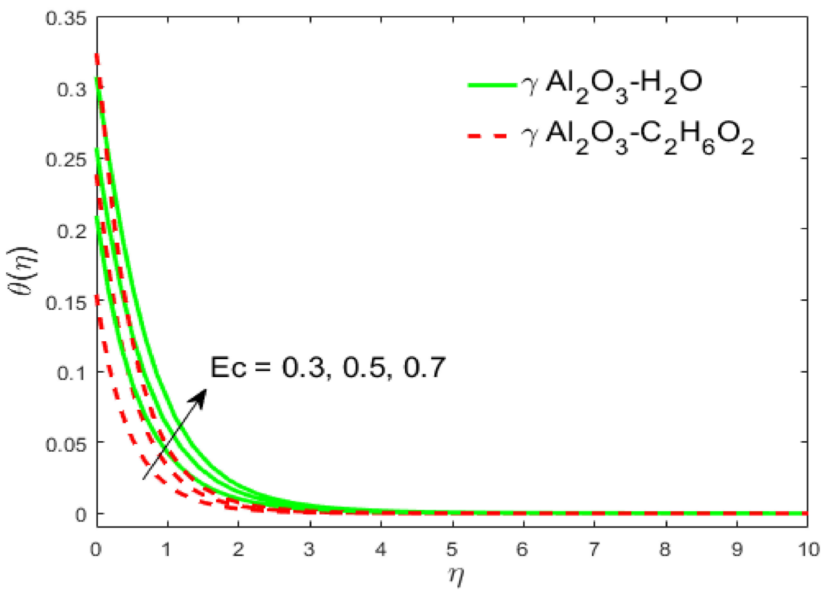

Figure 10. Impact of Ec on $\theta(\eta)$.

The sheet temperature gradient increases due to commanding convective heating. This permits the thermal influence to penetrate deeper in the sluggish fluid. Thus, the temperature increases. Figures 12 and 13 demonstrate the influence of heat sink/source on the $\theta(\eta)$ profile. It is clear from these profiles that the heat source increases the temperature, while the heat sink reduces the temperature, as expected.

Physically, the impact of the heat source $(A_0 > 0, B_0 > 0)$ adds extra energy within the boundary layer, which ultimately increases the temperature, while the heat sink $(A_0 < 0, B_0 < 0)$ absorbs the energy, which causes a reduction in the temperature.

Figures 14–16 illustrate the behavior of entropy generation for distinct parameters ϕ, Re_L and Br for $H_2O\backslash C_2H_6O_2$ based $\gamma - Al_2O_3$ nanofluids. Figure 14a,b show that the entropy increases due to ϕ in both nanofluids. It is interesting to note that ethylene-glycol-based nanofluid has greater impact on the entropy due to the huge Prandtl number and lower thermal diffusivity. Figure 15a,b suggest that the entropy enhances due to Re_L in both nanofluids owing to friction nanofluid and heat transport within the boundary layer for $\gamma Al_2O_3 - C_2H_6O_2$ and as well as $\gamma Al_2O_3 - H_2O$ nanofluids. Similarly, the impact of $\gamma Al_2O_3 - C_2H_6O_2$ on the entropy is greater than $\gamma Al_2O_3 - H_2O$. Figure 16a,b confirm that the entropy depicts the growing function of Br due to fluid friction for both nanofluids.

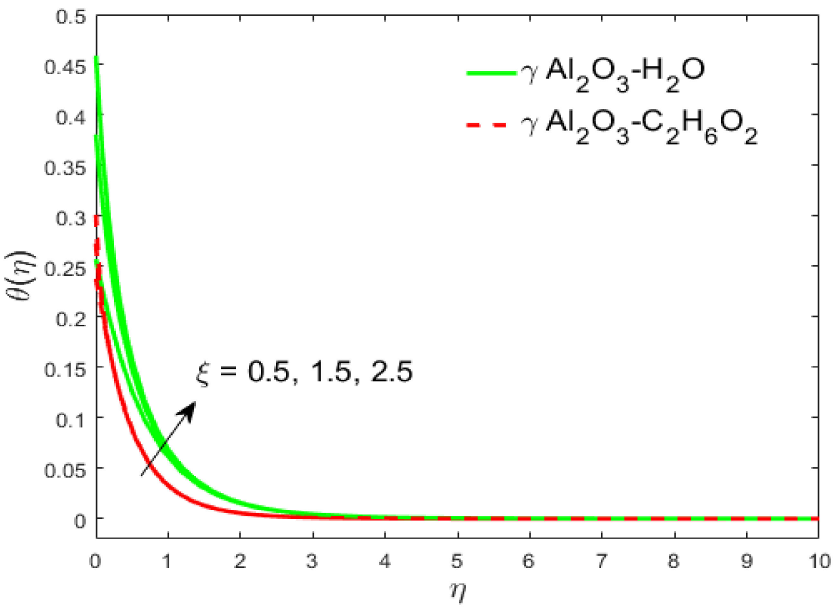

Figure 11. Impact of ξ on $\theta(\eta)$.

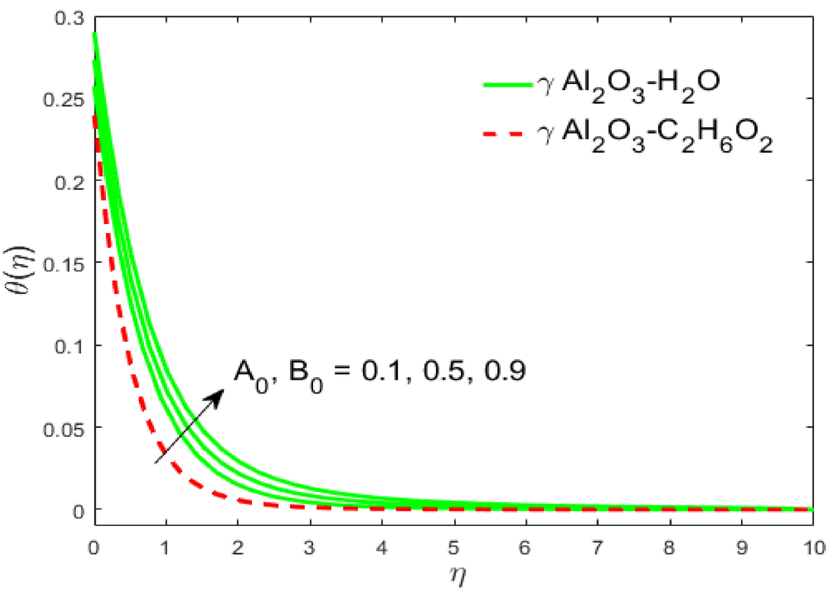

Figure 12. Impact of $A_0 > 0$, $B_0 > 0$ on $\theta(\eta)$.

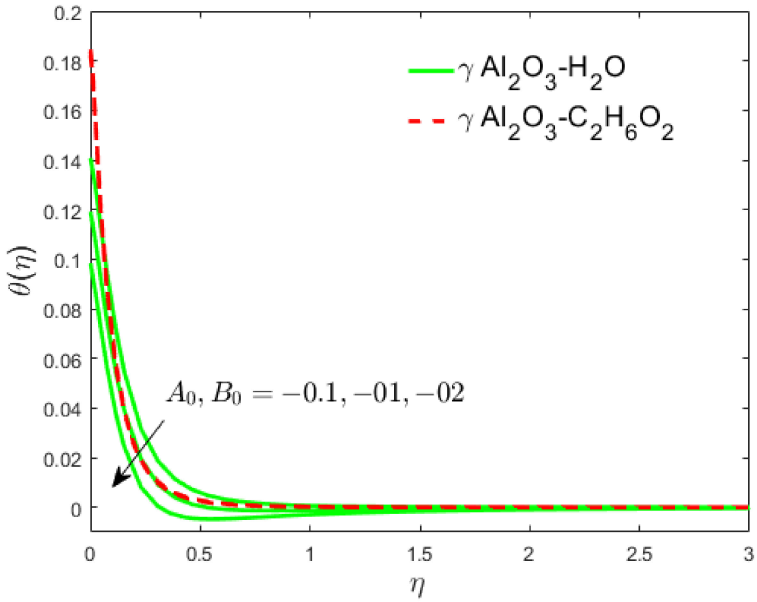

Figure 13. Impact of $A_0 < 0,\ B_0 < 0$ on $\theta(\eta)$.

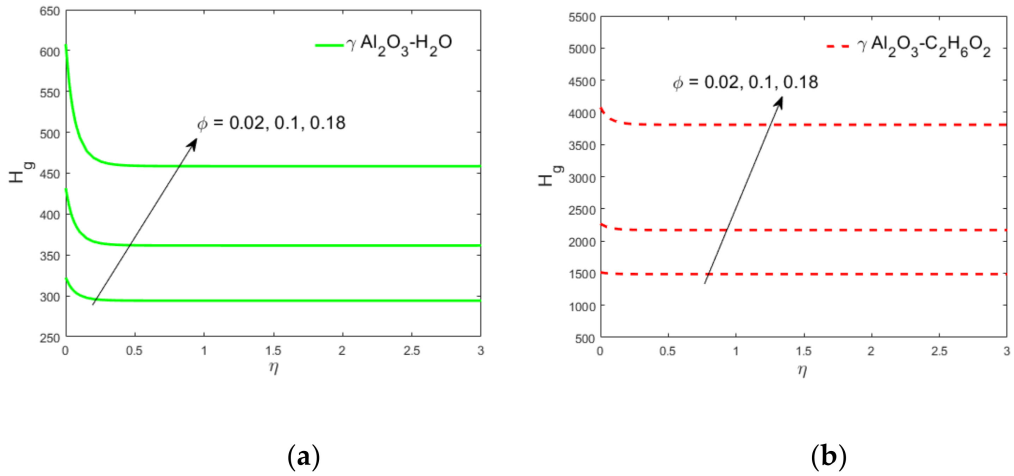

Figure 14. Impact of ϕ on EG (**a**) $\gamma - Al_2O_3 - H_2O$; (**b**) $\gamma - Al_2O_3 - C_2H_6O_2$.

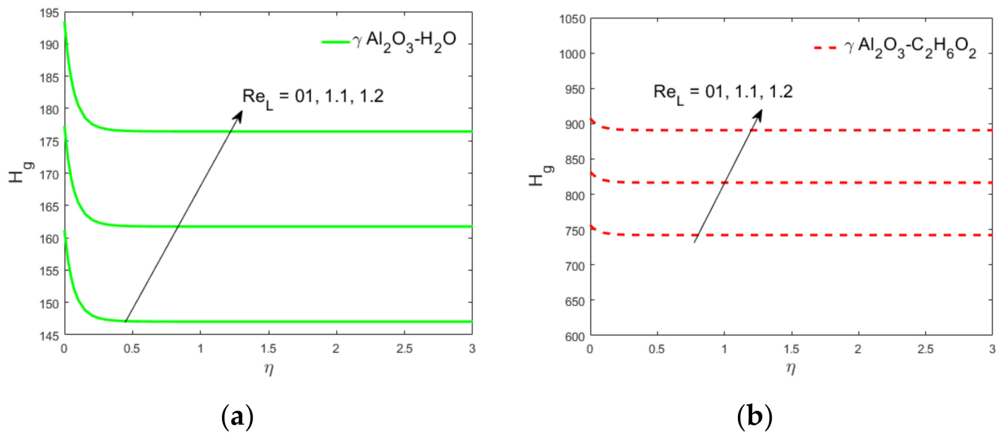

Figure 15. Impact of Re_L on EG (**a**) $\gamma - Al_2O_3 - H_2O$; (**b**) $\gamma - Al_2O_3 - C_2H_6O_2$.

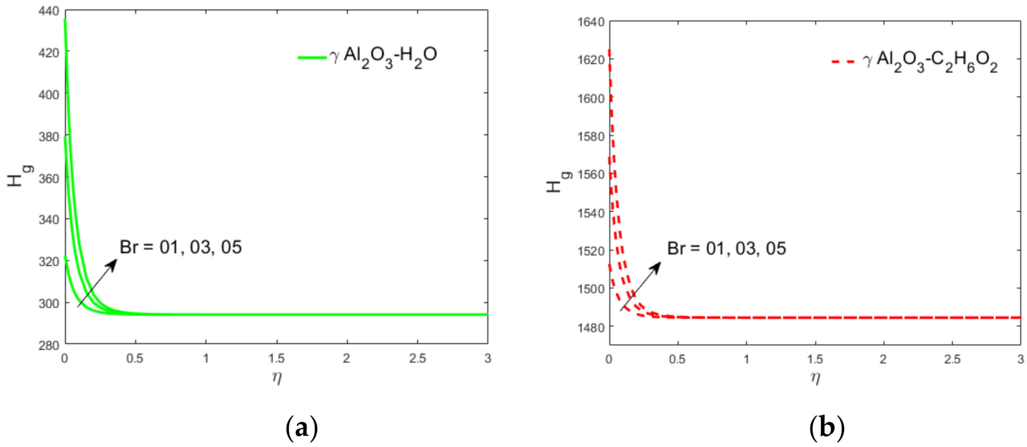

Figure 16. Impact of *Br* on EG. (**a**) $\gamma - Al_2O_3 - H_2O$; (**b**) $\gamma - Al_2O_3 - C_2H_6O_2$.

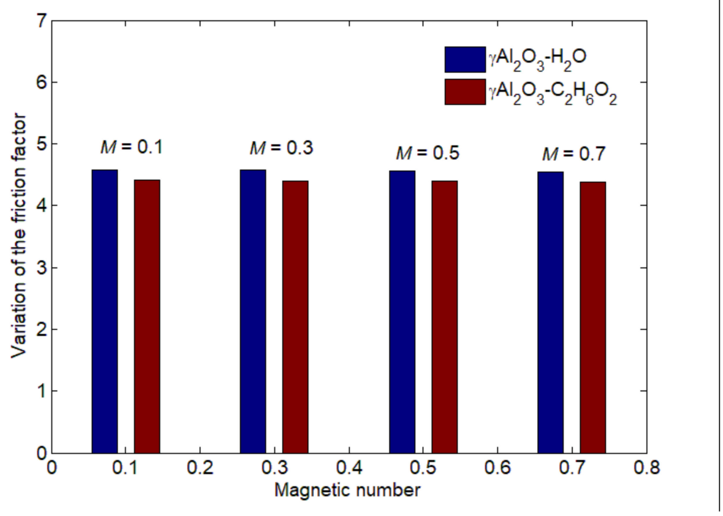

Figure 17. Impact of *M* on the friction factor.

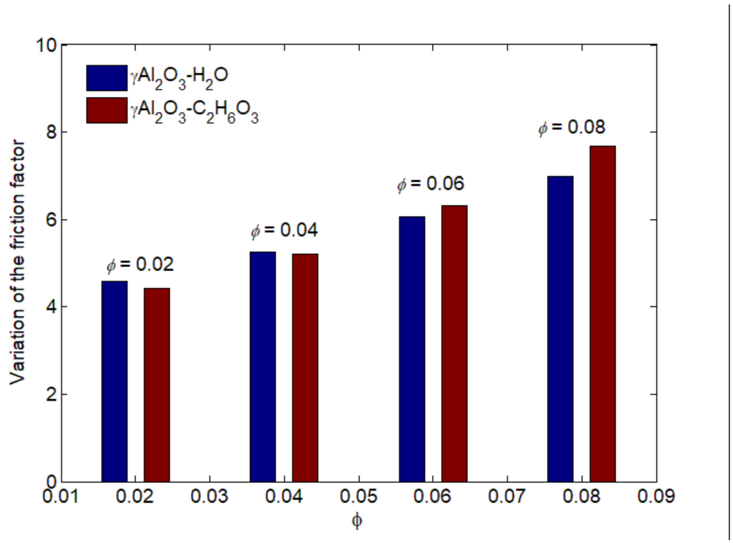

Figure 18. Impact of ϕ on the friction factor.

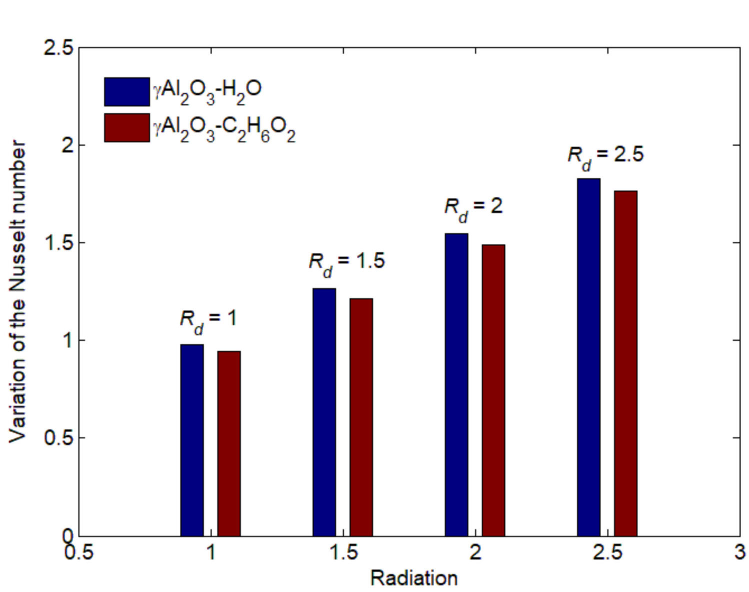

Figure 19. Impact of R_d on the Nusselt number.

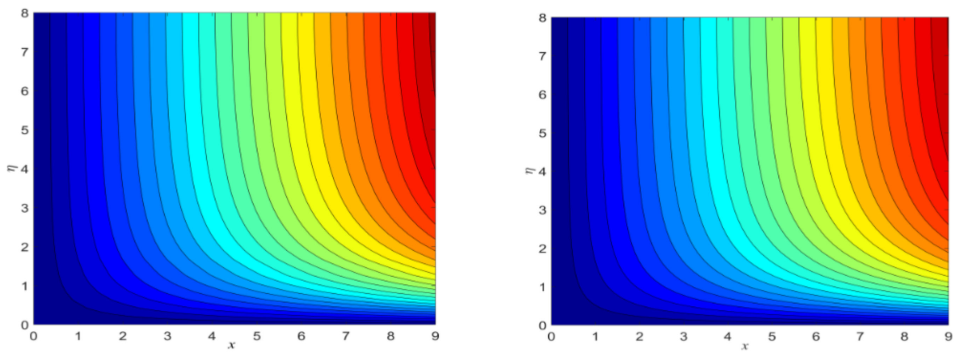

(**a**) (**b**)

Figure 20. The streamline patterns for (**a**) $\gamma Al_2O_3 - H_2O$ and (**b**)$\gamma Al_2O_3 - C_2H_6O_2$.

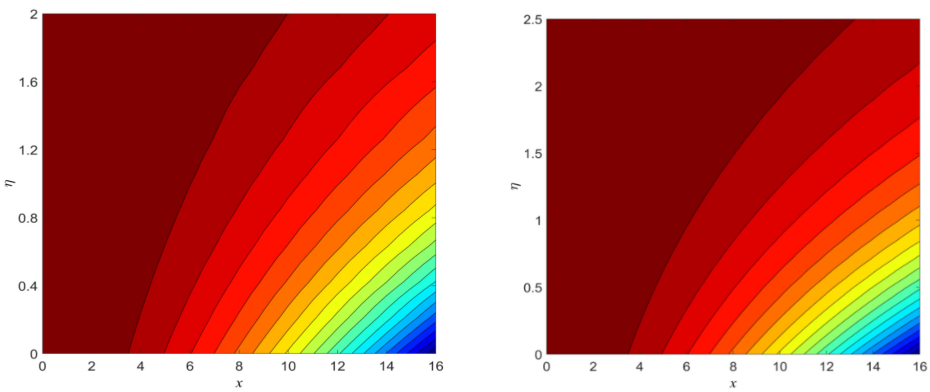

(**a**) (**b**)

Figure 21. The isotherm patterns for (**a**) $\gamma Al_2O_3 - H_2O$ and (**b**)$\gamma Al_2O_3 - C_2H_6O_2$.

The trend of significant parameters versus $\mathrm{Re}_x^{0.5} C_F$ and $\mathrm{Re}_x^{-0.5} Nu_x$ for $\gamma Al_2O_3 - C_2H_6O_2$ and $\gamma Al_2O_3 - H_2O$ is seen in Tables 6 and 7.

Table 6. The numerical values of $-\mathrm{Re}_x^{0.5}C_F$ when $\lambda = 0.1$.

M	ϕ	ε	$\gamma Al_2O_3-H_2O$	$\gamma Al_2O_3-C_2H_6O_2$
0.1	0.02	20	4.5829845	4.4160221
0.3			4.5707333	4.4041249
0.5			4.5584526	4.3921989
0.7			4.5461423	4.3802439
1.0			4.5276209	4.3622570
0.1	0.02	20	4.5829845	4.4160221
	0.04		5.2573609	5.2056061
	0.06		6.0648884	6.3245067
	0.08		6.9803698	7.6700892
	0.1		7.9850461	9.1769811
0.1	0.02	10	3.3254211	3.2044599
		20	4.5829845	4.4160221
		30	5.5632504	5.3605209
		40	6.3949900	6.1619350
		50	7.1303482	6.8705020

Table 7. The numerical values of $\mathrm{Re}_x^{-0.5}Nu_x$ when $\lambda = 0.1$.

R_d	Ec	ξ	θ_w	ϕ	ε	A_0	B_0	$\gamma Al_2O_3-H_2O$	$\gamma Al_2O_3-C_2H_6O_2$
01	0.5	0.5	01	0.02	20	0.1	0.1	0.979491227	0.941840165
1.5								1.26149515	1.21399674
02								1.54320424	1.48697783
2.5								1.8244553	1.76065943
3								2.10515155	2.03495597
01	0.3	0.5	01	0.02	20	0.1	0.1	1.03436938	1.02798261
	0.5							0.979491227	0.941840165
	0.7							0.924639087	0.85574787
	1.0							0.842404491	0.726703157
	1.5							0.70546786	0.511879004
01	0.5	0.5						0.979491227	0.941840165
		0.7						1.34834268	1.31435685
-	-	0.9						1.70505352	1.68449696
		1.1						2.05020822	2.05228348
		1.3						2.38436703	2.41773846
01	0.5	0.5	01	0.02	20	0.1	0.1	0.979491227	0.941840165
-	-	-	1.5					1.12509328	1.11333832
			2.0					1.29538442	1.27500857
			2.5					1.4938953	1.46547383
			3.0					1.72502842	1.81713438

Table 7. *Cont.*

R_d	Ec	ξ	θ_w	ϕ	ε	A_0	B_0	$\gamma Al_2O_3-H_2O$	$\gamma Al_2O_3-C_2H_6O_2$
01	0.5	0.5	01	0.02	20	0.1	0.1	0.979491227	0.941840165
				0.04				0.966302546	0.923406415
				0.06				0.952597644	0.909005851
				0.08				0.939634672	0.899736613
				0.10				0.927963377	0.894148357
01	0.5	0.5	01	0.02	10	0.1	0.1	0.962640123	0.937765787
					20			0.979491227	0.941840165
					30			0.98737614	0.943605729
					40			0.992183202	0.944638809
					50			0.995503652	0.945338938
01	0.5	0.5	01	0.02	20	0.1	0.1	0.979491227	0.941840165
						0.3	0.3	0.9788224	0.941810969
						0.5	0.5	0.978152778	0.94178177
						0.7	0.7	0.97748236	0.941752571
						0.9	0.9	0.976811145	0.941723371
01	0.5	0.5	01	0.02	20	−0.1	−0.1	0.980159261	0.941869361
						−0.3	−0.3	0.980826503	0.941898555
						−0.5	−0.5	0.981492955	0.941927748
						−0.7	−0.7	0.982158618	0.94195694
						−0.9	−0.9	0.982823494	0.94198613

In addition, bar diagrams are also shown in Figures 17–19.

It is concluded from these observations that the larger values of M subdued the friction factor in both nanofluids. The major reason is that MF capitulates the flow of nanofluids through the surface of the sheet owing to the prominent magnetic impact, which subdues the friction factor. In addition, the friction factor increases owing to the ϕ in both nanofluids. In the water-based $\gamma - Al_2O_3$ nanofluid, the values of the skin factor are greater compared to the ethylene-based $\gamma - Al_2O_3$ nanofluid, due to the superior thermal diffusivity. Moreover, the Nusselt number increases with the radiation due to fact that the radiation generates superior molecular force in the flow, while the opposite trend is explored due to the Eckert number. Both the Nusselt number and the friction factor increase due to the time-dependent parameter. The streamlines and isotherms are plotted in Figure 20a,b and Figure 21a,b.

6. Conclusions

In this article we examined the time-dependent flow for an effective Prandtl model of γ nanofluids from a stretched sheet. Mixed convection, nonlinear radiation and viscous dissipation were analyzed. The significant findings are listed below:

- Both profiles of velocity and the temperature increase owing to ϕ for $\gamma Al_2O_3 - H_2O\backslash C_2H_6O_2$ nanofluids.
- The velocity increases due to the assisting flow and decline in the opposing flow for $\gamma Al_2O_3 - H_2O\backslash C_2H_6O_2$ nanofluids, while the reverse trend is seen for temperature.
- The magnetic function decreases the velocity and increases the temperature distribution.
- The temperature of nanofluids increases due to radiation, Eckert, heat source and convective parameters, while the temperature decreases due to the heat sink.

- The EG increases due to Re_L, ϕ and Br for $\gamma Al_2O_3 - C_2H_6O_2$ and $\gamma Al_2O_3 - H_2O$ nanofluids.
- The influence of ethylene-glycol-based $\gamma - Al_2O_3$ nanofluids on the temperature is lesser compared to water-based $\gamma - Al_2O_3$ nanofluids.
- The friction factor decreases due to M and increases due to ϕ in both nanofluids.
- The Nusselt number increases due to R_d and declines due to Ec in both nanofluids.
- The time-dependent parameter increases the Nusselt number as well as the friction factor.

Author Contributions: Conceptualization, A.Z. and I.K.; methodology, U.K.; software, U.K.; validation, K.S.N., I.K. and U.K.; formal analysis, A.Z.; investigation, U.K.; resources, I.K.; data curation, U.K.; writing—original draft preparation, A.Z.; writing—review and editing, I.K.; visualization, K.S.N.; supervision, K.S.N.; project administration, I.K.; funding acquisition, K.S.N. All authors have read and agreed to the published version of the manuscript.

Funding: The authors did not receive any specific funding for this work.

Data Availability Statement: Data is contained within the article.

Conflicts of Interest: The authors declare that there is no conflict of interest regarding the publication of this paper.

References

1. Crane, L.J. Flow past a stretching plate. *Zeitschrift für angewandte Mathematik und Physik* **1970**, *21*, 645–647. [CrossRef]
2. Afzal, N.; Varshney, I.S. The cooing of a low heat resistance stretching sheet moving through a fluid. *Warme Stoffubertrag* **1980**, *14*, 289–293. [CrossRef]
3. Ali, M.E. Heat transfer characteristics of a continuous stretching surface. *Heat Mass Transf.* **1994**, *29*, 227–234. [CrossRef]
4. Andersson, H.; Bech, K.; Dandapat, B. Magnetohydrodynamic flow of a power-law fluid over a stretching sheet. *Int. J. Non-linear Mech.* **1992**, *27*, 929–936. [CrossRef]
5. Magyari, E.; Keller, B. Exact solutions for self-similar boundary-layer flows induced by permeable stretching walls. *Eur. J. Mech.—B/Fluids* **2000**, *19*, 109–122. [CrossRef]
6. Sparrow, E.M.; Abraham, J.P. Universal solutions for the streamwise variation of the temperature of a moving sheet in the presence of a moving fluid. *Int. J. Heat Mass Transf.* **2005**, *48*, 3047–3056. [CrossRef]
7. Abraham, J.P.; Sparrow, E.M. Friction drag resulting from the simultaneous imposed motions of a free stream and its bounding surface. *Int. J. Heat Fluid Flow* **2005**, *26*, 289–295. [CrossRef]
8. Ishak, A.; Nazar, R.; Pop, I. Boundary layer flow and heat transfer over an unsteady stretching vertical surface. *Meccanica* **2008**, *44*, 369–375. [CrossRef]
9. Zaib, A.; Sharidan, S. Thermal diffusion and diffusion thermo effects on unsteady MHD free convection flow over a stretching surface considering Joule heating and viscous dissipation with thermal stratification, chemical reaction and Hall current. *J. Franklin Inst.* **2004**, *351*, 1268–1287. [CrossRef]
10. Choi, S.U.S. Enhancing thermal conductivity of fluids with nanoparticles. In Proceedings of the ASME International Mechanical Engineering Congress and Exposition, San Francisco, CA, USA, 12–17 November 1995; pp. 99–105.
11. Sheikholeslami, M.; Mustafa, M.T.; Ganji, D.D. Effect of Lorentz forces on forced convection nanofluid flow over a stretched surface. *Particuology* **2016**, *26*, 108–113. [CrossRef]
12. Mutuku, W.N.; Makinde, O.D. Double stratification effects on heat and mass transfer in unsteady MHD nanofluid flow over a flat surface. *Asia Pac. J. Comput. Eng.* **2017**, *4*. [CrossRef]
13. Khan, N.S.; Gul, T.; Islam, S.; Khan, I.; Alqahtani, A.M.; Alshomrani, A.S. Magneto-hydrodynamic nanoliquid thin film sprayed on a stretching cylinder with heat transfer. *Appl. Sci.* **2017**, *7*, 271. [CrossRef]
14. Gireesha, B.; Mahanthesh, B.; Thammanna, G.; Sampathkumar, P. Hall effects on dusty nanofluid two-phase transient flow past a stretching sheet using KVL model. *J. Mol. Liq.* **2018**, *256*, 139–147. [CrossRef]
15. Soomro, F.A.; Zaib, A.; Haq, R.U.; Sheikholeslami, M. Dual nature solution of water functionalized copper nanoparticles along a permeable shrinking cylinder: FDM approach. *Int. J. Heat Mass Transf.* **2019**, *129*, 1242–1249. [CrossRef]
16. Mahanthesh, B.; Lorenzini, G.; Oudina, F.M.; Animasaun, I.L. Significance of exponential space- and thermal-dependent heat source effects on nanofluid flow due to radially elongated disk with Coriolis and Lorentz forces. *J. Therm. Anal. Calorim.* **2019**, *141*, 37–44. [CrossRef]
17. Eid, M.R. Effects of NP Shapes on Non-Newtonian Bio-Nanofluid Flow in Suction/Blowing Process with Convective Condition: Sisko Model. *J. Non-Equilibrium Thermodyn.* **2020**, *45*, 97–108. [CrossRef]
18. Khan, W.A.; Ali, M.; Shahzad, M.; Sultan, F.; Irfan, M.; Asghar, Z. A note on activation energy and magnetic dipole aspects for Cross nanofluid subjected to cylindrical surface. *Appl. Nanosci.* **2019**, *10*, 3235–3244. [CrossRef]

19. Kumar, P.B.S.; Gireesha, B.J.; Mahanthesh, B.; Chamkha, A.J. Thermal analysis of nanofluid flow containing gyrotactic microorganisms in bioconvection and second-order slip with convective condition. *J. Therm. Anal. Calorim.* **2019**, *136*, 1947–1957. [CrossRef]
20. Kumar, K.G.; Rahimi-Gorji, M.; Reddy, M.G.; Chamkha, A.J.; Alarifi, I.M. Enhancement of heat transfer in a convergent/divergent channel by using carbon nanotubes in the presence of a Darcy-Forchheimer medium. *Microsyst. Technol.* **2019**, *26*, 323–332. [CrossRef]
21. Maïga, S.E.B.; Nguyen, C.T.; Galanis, N.; Roy, G. Heat transfer behaviours of nanofluids in a uniformly heated tube. *Superlattices Microstruct.* **2004**, *35*, 543–557. [CrossRef]
22. Maiga, S.E.B.; Nguyen, C.T.; Galanis, N.; Roy, G.C. Micro and nano heat transfer heat transfer enhancement in forced convection laminar tube flow by using nanofluids. In Proceedings of the CHT-04—Advances in Computational Heat Transfer III. Proceedings of the Third International Symposium, Begell House, Danbury, CT, USA, 2004; p. 24.
23. Maïga, S.E.B.; Palm, S.J.; Nguyen, C.T.; Roy, G.; Galanis, N. Heat transfer enhancement by using nanofluids in forced convection flows. *Int. J. Heat Fluid Flow* **2005**, *26*, 530–546. [CrossRef]
24. Pop, C.V.; Fohanno, S.; Polidori, G.; Nguyen, C.T. Analysis of laminar-to-turbulent threshold with water γAl2O3 and ethylene glycol-γ γAl2O3 nanofluids in free convection. In Proceedings of the 5th IASME/WSEAS Int. Conference on Heat Transfer, Thermal Engineering and Environment, Athens, Greece, 25–27 August 2007; p. 188.
25. Farajollahi, B.; Etemad, S.; Hojjat, M. Heat transfer of nanofluids in a shell and tube heat exchanger. *Int. J. Heat Mass Transf.* **2010**, *53*, 12–17. [CrossRef]
26. Sow, T.M.O.; Halelfadl, S.; Lebourlout, S.; Nguyen, C.T. Experimental study of the freezing point of γ-Al2O3water nanofluid. *Adv. Mech. Eng.* **2012**, *4*, 162961. [CrossRef]
27. Maciver, D.S.; Tobin, H.H.; Barth, R.T. Catalytic aluminas I. Surface chemistry of eta and gamma alumina. *J. Catal.* **1963**, *2*, 487–497. [CrossRef]
28. Rashidi, M.M.; Ganesh, N.V.; Hakeem, A.K.A.; Ganga, B.; Lorenzini, G. Influences of an effective Prandtl number model on nano boundary layer flow of γAl2O3–H2O andγAl2O3–C2H6O2 over a vertical stretching sheet. *Int. J. Heat Mass Transf.* **2016**, *98*, 616–623. [CrossRef]
29. Ganesh, N.V.; Hakeem, A.A.; Ganga, B. A comparative theoretical study on Al2O3 and γ-Al2O3 nanoparticles with different base fluids over a stretching sheet. *Adv. Powder Technol.* **2016**, *27*, 436–441. [CrossRef]
30. Moghaieb, H.S.; Abdel-Hamid, H.M.; Shedid, M.H.; Helali, A.B. Engine cooling using γAl2O3/water nanofluids. *Appl. Therm. Eng.* **2017**, *115*, 152–159. [CrossRef]
31. Ahmed, N.; Adnan; Khan, U.; Mohyud-Din, S.T. A theoretical investigation of unsteady thermally stratified flow of γAl2O3–H2O and γAl2O3–C2H6O2 nanofluids through a thin slit. *J. Phys. Chem. Solids* **2018**, *119*, 296–308. [CrossRef]
32. Zaib, A.; Haq, R.; Sheikholeslami, M.; Khan, U. Numerical analysis of effective Prandtl model on mixed convection flow of γAl2O3–H2O nanoliquids with micropolar liquid driven through wedge. *Phys. Scr.* **2019**, *95*, 035005. [CrossRef]
33. Bejan, A. *Entropy Generation Minimization: The Method of Thermodynamic Optimization of Finite-Size Systems and Finite-Time Processes*, 1st ed.; CRC Press; Taylor & Francis: Boca Raton, FL, USA; ISBN 97814987829201996.
34. Bejan, A. A Study of Entropy Generation in Fundamental Convective Heat Transfer. *J. Heat Transf.* **1979**, *101*, 718–725. [CrossRef]
35. Ko, T.; Ting, K. Optimal Reynolds number for the fully developed laminar forced convection in a helical coiled tube. *Energy* **2006**, *31*, 2142–2152. [CrossRef]
36. Hajmohammadi, M.R.; Lorenzini, G.; Shariatzadeh, O.J.; Biserni, C. Evolution in the Design of V-Shaped Highly Conductive Pathways Embedded in a Heat-Generating Piece. *J. Heat Transf.* **2015**, *137*, 061001. [CrossRef]
37. Xie, G.; Song, Y.; Asadi, M.; Lorenzini, G. Optimization of Pin-Fins for a Heat Exchanger by Entropy Generation Minimization and Constructal Law. *J. Heat Transf.* **2015**, *137*, 061901. [CrossRef]
38. Lorenzini, G.; Moretti, S. Bejan's Constructal theory and overall performance assessment: The global optimization for heat exchanging finned modules. *Therm. Sci.* **2014**, *18*, 339–348. [CrossRef]
39. Abouzar, P.; Hajmohammadi, M.R.; Sadegh, P. Investigations on the internal shape of constructal cavities intruding a heat generating body. *Therm. Sci.* **2015**, *19*, 609–618.
40. Hajmohammadi, M.R.; Campo, A.; Nourazar, S.S.; Ostad, A.M. Improvement of Forced Convection Cooling Due to the Attachment of Heat Sources to a Conducting Thick Plate. *J. Heat Transf.* **2013**, *135*, 124504. [CrossRef]
41. Govindaraju, M.; Ganesh, N.V.; Ganga, B.; Hakeem, A.A. Entropy generation analysis of magneto hydrodynamic flow of a nanofluid over a stretching sheet. *J. Egypt. Math. Soc.* **2015**, *23*, 429–434. [CrossRef]
42. Rashidi, M.; Abelman, S.; Mehr, N.F. Entropy generation in steady MHD flow due to a rotating porous disk in a nanofluid. *Int. J. Heat Mass Transf.* **2013**, *62*, 515–525. [CrossRef]
43. Dalir, N.; Dehsara, M.; Nourazar, S.S. Entropy analysis for magnetohydrodynamic flow and heat transfer of a Jeffrey nanofluid over a stretching sheet. *Energy* **2015**, *79*, 351–362. [CrossRef]
44. Shit, G.C.; Haldar, R.; Mandal, S. Entropy generation on MHD flow and convective heat transfer in a porous medium of ex-ponentially stretching surface saturated by nanofluids. *Adv. Powder Tech.* **2017**, *28*, 1519–1530. [CrossRef]
45. Hayat, T.; Khana, M.I.; Qayyuma, S.; Alsaedi, A. Entropy generation in flow with silver and copper nanoparticles. *Colloids Surfaces* **2018**, *539*, 335–346. [CrossRef]

46. Shafee, A.; Jafaryar, M.; Alsabery, A.I.; Zaib, A.; Babazadeh, H. Entropy generation of nanomaterial through a tube considering swirl flow tools. *J. Therm. Anal. Calorim.* **2020**, 1–16. [CrossRef]
47. Ganesh, N.V.; Chamkha, A.J.; Al-Mdallal, Q.M.; Kameswaran, P.K. Magneto-Marangoni nano-boundary layer flow of water and ethylene glycol based γAl2O3 nanofluids with non-linear thermal radiation effects. *Case Stud. Thermal Eng.* **2018**, *12*, 340–348.
48. Makinde, O.D.; Olanrewaju, P.O. Buoyancy Effects on Thermal Boundary Layer Over a Vertical Plate With a Convective Surface Boundary Condition. *J. Fluids Eng.* **2010**, *132*, 044502. [CrossRef]
49. Shafie, S.; Mahmood, T.; Pop, I. Similarity solutions for the unsteady boundary layer flow and heat transfer due to a stretching sheet. *Int. J. Appl. Mech. Eng.* **2006**, *11*, 647–654.
50. Chamkha, A.J.; Aly, A.M.; Mansour, M.A. Similarity solution for unsteady heat and mass transfer from a stretching surface embedded in a porous medium with suc-tion/injection and chemical reaction effects. *Chem. Eng. Commun.* **2010**, *197*, 846–858. [CrossRef]